# A Technique for Enhancing and Matching the Resolution of Microwave Measurements from the SSM/I Instrument

Wayne D. Robinson, Christian Kummerow, and William S. Olson

## I. Introduction

Satellite-based, multispectral measurements of the atmosphere are often plagued with the problem of nonuniform spatial resolutions available at the various frequencies. This problem is especially critical in the microwave portion of the spectrum where diffraction limits the attainable resolution. The currently available microwave data from the Special Sensor Microwave/Imager (SSM/I) spans frequencies from 19.35 GHz with 55-km horizontal resolution, to 85.5 GHz with 12.5-km resolution. This mismatch in resolution becomes a critical consideration when observations at many frequencies must be combined to retrieve single parameters which are not generally homogeneous over such large dimensions. Examples of such parameters which can be retrieved from the SSM/I include cloud water, precipitation, soil moisture, and snow cover. Channel combination techniques for the retrieval of such parameters are, therefore, not strictly valid unless steps are taken to match the different resolutions.

The obvious solution to this problem is to average the higher resolution measurements to match the lower resolution data. This solution, however, is not very desirable when the relation between the geophysical parameter, such as rainfall, and the radiances is highly nonlinear. A much more desirable result would be to increase the spatial resolution of the low frequency channels to match the resolutions of the higher frequency channels. In this paper we describe and apply a correction technique for matching the resolution of all the frequencies of the SSM/I to the ~25-km spatial resolution of the 37-GHz channel. To accomplish this, it is necessary to increase the spatial resolution of the 19- and 22-GHz channels while degrading that of the 85-GHz channel.

The methodology for the correction technique was first proposed by Backus and Gilbert [1] in 1970, in connection with the inversion of gross Earth data. The technique was later applied by Stogryn [2] to satellite field of view problems. In essence, the theory contends that if the density of measurements made by the satellite is higher than the resolution of the instrument, then it is possible to find a linear combination of surrounding measurements which yield results at a higher spatial resolution than the original data. The trade-off for higher spatial resolution in this procedure is the rapid amplification of instrument noise. One immediate consequence is that for the retrieval of geophysical parameters from SSM/I measurements, noise amplification may render an increase of the common spatial resolution from that of the 37-GHz to the 85-GHz resolution infeasible.

The simpler problem of degrading the spatial resolution to the lowest common resolution has been applied to SSM/I data previously by Hollinger *et al.* [3]. The technique described in this paper does not constitute a breakthrough in the field of resolution enhancement. Instead, we are applying an existing theoretical framework to a current problem. Our goal is to obtain uniform spatial resolution for all the channels at the intermediate resolution of the 37-GHz channel, and to properly document the procedure and its results for the SSM/I instrument. Using real and simulated data, we have carefully detailed the actual achievable increase in the spatial resolution, as well as a quantitative estimate of the additional random noise introduced by this procedure. The calculated coefficients, available from the authors, can be of great value to those researchers who are using channel combination techniques for the retrieval of geophysical parameters.

Section II describes the SSM/I instrument and the correction technique in greater detail. Section III discusses the quantitative results obtained by applying the correction technique to simulated SSM/I data containing noise. Section IV discusses the results obtained when the correction technique is applied to actual SSM/I data. Finally, Section V summarizes our findings.

## II. Inversion of Radiance Measurements

The Special Sensor Microwave/Imager (SSM/I) instrument is a conically scanning microwave radiometer flying aboard the current DMSP spacecraft series. It is described in more detail in the SSM/I User's Guide [3]. The instrument flies at an altitude of 833 km and scans the earth in a conical scan 1400 km wide. The SSM/I samples data in seven channels covering four microwave frequencies (see Table I). The lower frequencies of the instrument (19.35, 22.235, and 37.0 GHz.) are sampled every 25 km along the scan and every 25 km along the track while the higher frequency (85.5 GHz) is sampled every 12.5 km. The four frequencies are sampled in both the horizontal and vertical polarizations except the 22 GHz which

Manuscript received September 13, 1990; revised July 1, 1991; rerevised November 25, 1991.

W. D. Robinson is with the General Sciences Corporation, Laurel, MD 20707.

C. Kummerow is with the Laboratory for Atmospheres, Goddard Space Flight Center, Greenbelt, MD 20771.

W. S. Olson is with the Cooperative Institute for Meteorological Satellite Studies, University of Wisconsin, Madison, WI 53705.

IEEE Log Number 9107035.

TABLE I
SPATIAL RESOLUTION OF SSM/I CHANNELS. ADAPTED FROM HOLLINGER *ET AL.* [3]

| Frequency (GHz) | Polarization | Resolution Along-track (km) | Resolution Cross-track (km) | Spatial sampling (km) | Noise $\Delta T$ (K) |
|---|---|---|---|---|---|
| 19.35 | horizontal | 69 | 43 | 25 | .42 |
| 19.35 | vertical | 69 | 43 | 25 | .45 |
| 22.235 | vertical | 50 | 40 | 25 | .74 |
| 37.0 | horizontal | 37 | 29 | 25 | .38 |
| 37.0 | vertical | 37 | 28 | 25 | .37 |
| 85.5 | horizontal | 15 | 13 | 12.5 | .73 |
| 85.5 | vertical | 51 | 13 | 12.5 | .69 |

is sampled in the vertical polarization only. The seven channels will be referred to as 19H, 19V, 22V, 37H, 37V, 85H, and 85V.

The purpose of this section is to provide a basic framework for the resolution enhancement technique. The resolution enhancement technique was developed by Backus and Gilbert [1], [4], [5] to invert seismic observations to produce detailed profiles of the earth's density structure. In [1], the theory was fully developed, taking into account observation noise. Stogryn [2] later adapted the technique to the inversion of microwave measurements by the Electronically Scanning Microwave Radiometer (ESMR-5). Because much of the theory for the current problem has been addressed in the cited literature, no effort is made here to develop the theories fully. Instead, this section is intended to serve as a starting point for readers not familiar with these theories, and to set forth notation.

The brightness temperature, $Ta(\boldsymbol{s}_0, \nu, \boldsymbol{p})$ seen by the SSM/I antenna at any given frequency, $\nu$, and polarization $\boldsymbol{p}$, at location $\boldsymbol{s} = \boldsymbol{s}_0$, is the convolution of the actual scene brightness temperature, $Tb(\boldsymbol{s}, \nu, \boldsymbol{p})$ with the antenna response or gain function $G(\boldsymbol{s}_0, \boldsymbol{s})$. Here, and throughout the rest of this paper, bold lettering is used to indicate vector quantities. Omitting the arguments $\nu$ and $\boldsymbol{p}$ to simplify the notation, this can be expressed as:

$$Ta(\boldsymbol{s}_0) = \int G(\boldsymbol{s}_0, \boldsymbol{s})\, Tb(\boldsymbol{s})\, dA. \tag{1}$$

Our general objective is to find the actual scene brightness temperature, $Tb(\boldsymbol{s})$, at the highest possible resolution, given the fact that there are a finite number of noisy measurements. Following [1], we assume that $Tb(\boldsymbol{s}_0)$ can be constructed from a linear combination of $N$ adjacent antenna brightness temperatures $Ta(\boldsymbol{s}_0)_i$, $i = 1, \ldots, N$. This can be written as:

$$Tb(\boldsymbol{s}) = \sum_{i=1}^{N} a_i\, Ta(\boldsymbol{s}_0)_i. \tag{2}$$

(1) and (2) may then be combined to yield:

$$Tb(\boldsymbol{s}_0) = \int [\sum_{i=1}^{N} a_i\, G_i(\boldsymbol{s}_0, \boldsymbol{s})]\, Tb(\boldsymbol{s})\, dA. \tag{3}$$

If one can find coefficients, $a_i$, such that the bracketed term in (3) becomes the Dirac-delta function $\delta(\boldsymbol{s}_0 - \boldsymbol{s})$, then (3) would be an exact solution to the problem, and (2) could be used to find the actual scene brightness temperature at any desired resolution. In practice, however, the finite number of measurements make it impossible to find such a set of coefficients, $a_i$.

Instead, we confine ourselves to selecting a set of coefficients, $a_i$, which cause the bracketed term in (3) to most closely produce some desired behavior. In particular, we will look for a set of coefficients, $a_i$, which make the bracketed term in (3) appear like the gain function $G(\boldsymbol{s}_0, \boldsymbol{s})$ of the 37-GHz channel. While this does not change (1)–(3), it must be understood that $Tb(\boldsymbol{s})$ is no longer the true scene brightness temperature, but the brightness temperature as it would be seen at the 37-GHz resolution. By using the actual 37-GHz antenna function as the match function, no correction is necessary for the 37-GHz channels. The use of a naturally occurring function as a match function further avoids the problems that can occur when matching to a function with sharp discontinuities. The 37-GHz antenna function also has a footprint which is most similar in size to the 25-km spatial sampling distance of the instrument.

Consider the quantity:

$$Q_0 = \int [\sum_{i=1}^{N} a_i\, G_i(\boldsymbol{s}_0, \boldsymbol{s}) - G^{37}(\boldsymbol{s}_0, \boldsymbol{s})]^2\, dA \tag{4}$$

where $G^{37}(\boldsymbol{s}_0, \boldsymbol{s})$ is the gain function of the 37-GHz channel. Minimizing $Q_0$ with respect to $a_i$, subject to the constraint that proper normalization be preserved,

$$\int \sum_{i=1}^{N} a_i\, G_i(\boldsymbol{s}_0, \boldsymbol{s})\, dA = 1. \tag{5}$$

should produce the best correction coefficients possible in the least square sense.

The above treatment assumes the antenna measurements to be exact. In practice, however, the antenna temperatures, $Ta_i(\boldsymbol{s}_0)$ will not be known exactly, but rather will contain some random noise whose variance is given by $(\Delta T_{\text{rms}})^2$. The estimate of $Tb(\boldsymbol{s})$ given by (3), and the fact that random errors in adjacent pixels are uncorrelated, implies that the variance of $Tb(\boldsymbol{s})$ due to noisy measurements can be expressed as:

$$e^2 = (\Delta T_{\text{rms}})^2 \sum_{i=1}^{N} a_i^2. \tag{6}$$

For our purposes, we want not only to increase the resolution of the 19- and 22-GHz measurements, but we also want to avoid introducing any drastic increases in the instrument noise. We thus seek a compromise between resolution and noise. Rather than minimizing $Q_0$ in (4), we therefore minimize

$$Q = Q_0 \cos\gamma + e^2 w \sin\gamma \tag{7}$$

where $w$ is a scale factor used to make the two terms on the right-hand side of (7) dimensionally and numerically compatible. We chose $w = 0.001$. In this formulation, $\gamma$ can be varied between 0 and $\pi/2$ to place various degrees of emphasis on either the resolution enhancement or the noise suppression in the estimate of $Tb(s)$. The procedure used to select the appropriate $\gamma$ is detailed in Section III. The details of solving for the coefficients $a_i$ can be found in both [1] and [2] and, consequently, will not be replicated here. The final result is given by:

$$\boldsymbol{a} = \boldsymbol{S}^{-1}[\boldsymbol{v}\cos\gamma - \lambda\boldsymbol{u}.] \tag{8}$$

where

$$\lambda = \frac{-1 + \boldsymbol{u}\,\boldsymbol{S}^{-}1\,\boldsymbol{v}\,\cos\gamma}{\boldsymbol{u}\,\boldsymbol{S}^{-}1\,\boldsymbol{u}} \tag{9}$$

and $S_{i,j}$, $u_i$, and $v_i$ are given by:

$$\begin{aligned} \boldsymbol{S}_{i,j} &= \cos\gamma \int G_i\, G_j\, dA + \delta_{i,j}\,(\Delta T_{\mathrm{rms}})^2\, w\, \sin\gamma \\ \boldsymbol{u}_i &= \int G_i\, dA \\ \boldsymbol{v}_i &= \int G^{37}\, G_i\, dA \end{aligned} \tag{10}$$

where the arguments of $G$ have been suppressed for clarity and $\delta_{ij}$ is the Kronecker delta function.

## III. Simulation Results

The enhancement technique is designed to produce 37-GHz resolution brightness temperature fields in all the SSM/I channels. Validation of the enhanced resolution fields directly from real SSM/I data is nearly impossible, since the response of the different channels to a given scene are different. One possible approach is to validate the enhanced image against an assumed "edge," which at the SSM/I frequencies occurs in the vicinity of coastlines. The main difficulty in this approach is that the specification of brightness temperatures in the vicinity of the coast can be difficult, since brightness variations (especially over land) can cause significant deviations from idealized "step-function" behavior at the coastal boundary. Simulated data, however, offers an excellent substitute. Since the antenna gain pattern is well known from preflight calibration work [3], it is possible to accurately simulate antenna responses to any desired brightness temperature field. Test data can be created from a known scene with known noise, allowing for quantitative results to be obtained on the performance of the correction method. Simulated data will therefore be used to find the proper value of the noise conditioning weighting factor, $\gamma$, and the total number of surrounding pixels, $N$, to be considered by the correction technique.

The SSM/I data are simulated on a square domain of 700 by 700 km with an observation spacing of 25 km for the 19-, 22-, and 37-GHz channels and 12.5 km for the 85-GHz channels. This regular grid best approximates the geometry of the central portion of the SSM/I scan where the across-track scan direction is perpendicular to the along-track scan direction. This portion of the scan was selected because the symmetry of pixels in this portion of the scan presents the greatest challenge to the correction technique. If noise amplification is properly constrained in this portion of the swath, then one can be confident that it is also properly constrained elsewhere in the scan. The actual scene consists of a circular feature with a radius of 169 km and black body temperature of 250 K centered in a background of 150 K. This scene is then convolved with the antenna function of a particular channel on a subgrid of 1 km resolution to produce the simulated scene as viewed by the antenna in that channel. Once the scene is simulated, noise is added to it which is characteristic of that channel. The noise values created have a Gaussian distribution with an RMS corresponding to the RMS measured for that channel (see Table I).

In creating the correction coefficients defined by (8), two parameters must be varied to determine the best correction method. The first parameter, $N$, is the number of observations that are used to perform the correction. In the tests done here, either a 3x3, a 5x5, or a 7x7 set of observations are used to correct the central observation. Larger numbers of observations should act to increase the quality of the correction due to the greater amount of information that can be drawn on. The second parameter that must be considered is the error conditioning weighting parameter $\gamma$. Without error conditioning, ambient noise would be interpreted as significant data to be corrected, resulting in the amplification of that noise. The choice of $\gamma$ must be made large enough to reduce the noise amplification in the correction but not so large as to result in no correction at all. With a value of 0.001 for $w$ in (7), simulated correction coefficients are generated for 10 values of $\gamma$ = between 0 and 30°. Note that because the 85-GHz channels are corrected by an averaging process which naturally reduces noise, the $\gamma$ value may remain at 0 for these channels.

The combination of these parameters results in a set of 30 tests to run on each of the three lower frequency channels and three tests on each of the 85-GHz channels of the SSM/I. Correction coefficients for each of these cases are applied to the simulated scene to create the corrected scene. If the correction is perfect, the corrected scene should match the scene simulated with the response function of the 37-GHz channel to within the RMS of the noise. To obtain a quantitative estimate for the performance of the correction technique, we define the RMS difference as the root mean square difference between the brightness temperatures of the channel under investigation and the brightness temperature field created with the 37-GHz response function over the entire scene. Because, in this definition, the RMS difference is scene dependent, and the RMS differences should be viewed only in terms of their relative sizes. Quantitative estimates of the improvement can now be made by comparing the RMS differences between corrections using various values of $N$ and $\gamma$ and the uncorrected RMS.

Fig. 1 shows the RMS difference between a corrected simulated field of SSM/I data and the simulated 37-GHz field of the same polarization for the 19H, 19V, and 22V channels. Each graph in Fig. 1 shows the RMS as a function

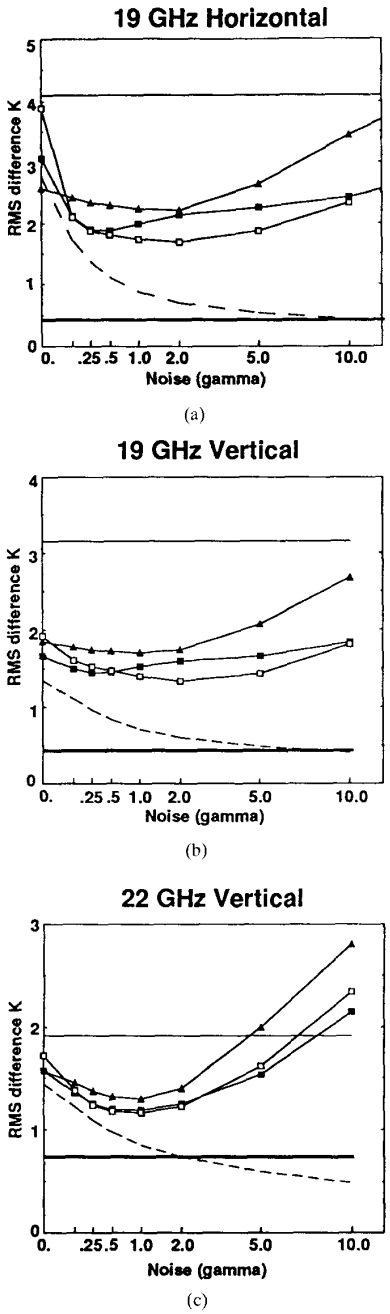


Fig. 1. Performance of the SSM/I resolution correction coefficients on a simulated scene as a function of noise conditioning and observation set size. Corrections were evaluated for the (a) 19H, (b) 19V, and (c) 22V channels. The performance is measured as the RMS difference between the corrected channel and the 37-GHz channel. A perfect correction would give an RMS difference of 0. Each graph shows the RMS as a function of the error conditioning factor, $\gamma$. The abscissa ($\gamma$), has been expanded at the low end to show more detail in the curves. The unlabeled tick mark between 0 and 0.25 is at $\gamma = 0.1$. The top thin horizontal line is the RMS before the correction was applied. The heavy line at the bottom is the noise component of the uncorrected channel. The three solid curves between these lines represent the RMS in the corrected field for observation set sizes of 3×3 (solid triangles), 5×5 (solid squares), and 7×7 (open squares), while the dotted curve represents the general trend of the noise component in those corrected fields.

of the error conditioning factor, $\gamma$. The abscissa ($\gamma$), has been expanded at the low end to show more detail in the curves. The top thin horizontal line is the RMS before the correction was applied. The heavy line at the bottom is the noise component of the uncorrected channel. The three solid curves between these lines represent the RMS in the corrected field for observation set sizes of 3×3, 5×5, and 7×7 while the dotted curve represents the general trend of the noise component in those corrected fields. The noise component is the instrument noise amplified by the enhancement technique, $e^2$ in (6). Frequently, the noise component curve is similar for the different observation set sizes over a wide range of $\gamma$ and is represented by one curve for simplicity in the figure.

The response of the RMS difference to the noise conditioning value is similar for all three channels and all observation set sizes. The RMS difference at $\gamma = 0$ shows some improvement of the simulated scene due to correction but most of the RMS is attributed to the growth of the noise. For example, in the 19H channel, the original RMS of 4.1 K is reduced to 2.6 K using the 3×3 correction with background noise accounting for 1.9 K. This is a significant growth in the noise over the uncorrected noise of 0.45 K. As $\gamma$ is increased, the background noise component decreases rapidly along with the RMS difference. At $\gamma = 2$, the RMS difference reaches a minimum of 2.2 K after which it slowly rises.

The background noise is decreased to 0.75 K at this point. For the 5×5 observation set, a similar trend occurs with a minimum in the RMS difference of 1.9 K occurring at $\gamma = 0.5$ and background noise of 1.1 K. The 7×7 observation set has a minimum RMS of 1.6 K at $\gamma = 2$ and a background noise of 0.74 K. Figs. 1(b) and (c) show similar behaviors of the data. The significant information relating to the minimum RMS value for each curve at each frequency is shown in Table II. The general trend for all the three lower frequency channels is for an improvement in the minimum RMS value as the number of observations in the correction set is increased.

In the case of both the 19H and V channels, the RMS minimum occurs at different values of $\gamma$ for the different observation set sizes. For the 5x5 correction, the minimum RMS difference occurs at relatively small values of $\gamma$, resulting in a larger, but acceptable noise component when compared to the 3x3 or 7×7 corrections. The RMS minimum for the 22V channel stays fixed at $\gamma = 1.0$ regardless of the observation set size used. Also, little improvement occurs in the minimum RMS for the 22V channel when the observation set size is increased from 5×5 to 7×7. In general, the greatest improvement came when a 3×3 correction was applied. This brought the RMS difference down by approximately one third. Further improvement was considerably less dramatic although still significant with the 5×5 and 7×7 observation sets.

Fig. 2 shows the RMS difference and the noise component for corrections applied to the 85H (Fig. 2(a)) and 85V (Fig. 2(b)) channels. Error conditioning is not tested because the noise is reduced by the correction procedure for this channel. The 85H and 85V channels show the best improvement of all the channels. This is to be expected as the correction process is reducing the resolution and the noise of these channels substantially. Figs. 2(a) and (b) show the original random noise

TABLE II
LOCATION OF THE BEST CORRECTION (MINIMUM RMS) FOR EACH OBSERVATION SET SIZE IN THE SIMULATION TESTS

| Channel, set size | | min RMS diff (K) | noise component (K) | $\gamma$ at minimum (° |
|---|---|---|---|---|
| 19H, | 1x1 | 4.10 | .45 | |
| | 3x3 | 2.21 | .75 | |
| | 5x5 | 1.88 | 1.11 | |
| | 7x7 | 1.69 | .73 | |
| 19V, | 1x1 | 3.10 | .45 | — |
| | 3x3 | 1.71 | .73 | 1.0 |
| | 5x5 | 1.45 | .96 | 0.25 |
| | 7x7 | 1.34 | .63 | 2.0 |
| 22V, | 1x1 | 1.92 | .75 | — |
| | 3x3 | 1.30 | .85 | 1.0 |
| | 5x5 | 1.19 | .85 | 1.0 |
| | 7x7 | 1.16 | .85 | 1.0 |

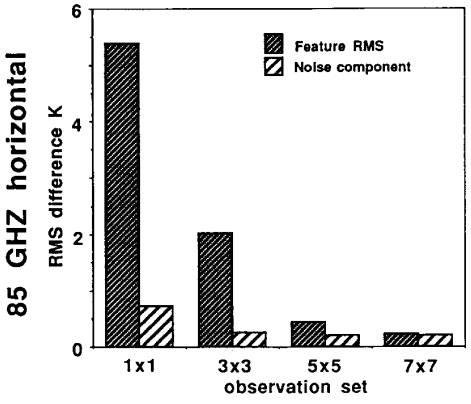


(a)

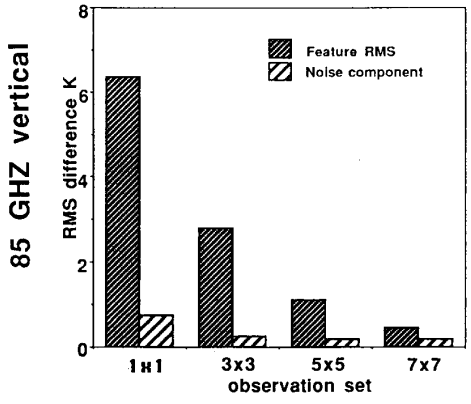


(b)

Fig. 2. Performance of the SSM/I resolution correction coefficients on a simulated feature as a function of observation set size. For each observation set from 1×1 (no correction) to 7×7, the RMS difference between the corrected simulated scene and the 37-GHz target scene is displayed for the (a) 85H and (b) 85V channels. Also displayed is the noise component of this difference.

of 0.73 K reduced to around 0.2 K when the correction is applied. The RMS difference for 85H dropped dramatically from 5.4 K uncorrected to 2 K with a 3×3 correction, 0.45 K with a 5×5 correction and 0.22 K with a 7×7 correction. Similar results were achieved with the 85V channel.

The numerical results show that significant corrections can be made to all the SSM/I channels in bringing them toward the same resolution of the 37-GHz channel. This improvement cannot be achieved without a significant increase in the noise component in the lower frequency channels. However, if less noise is desired, corrections can be obtained with minimal noise growth by increasing the conditioning factor, $\gamma$. A 7×7 observation set produced the best correction in all channels although the amount of improvement appears to decline as the observation set is increased beyond 3×3. For the 85-GHz channels, the 7×7 correction appears to almost fully correct (or average) the data to the 37-GHz target. The correction of the 85-GHz channels amounts to a simple, albeit the very best possible, averaging of the surrounding observations. Limitations on resources prohibit the exploration of corrections at higher observation set sizes but it is expected that little improvement in the corrections is possible due to the drop-off of the antenna functions and the corresponding lack of information further from the antenna boresight.

Images created from the corrected 19H field illustrate the effects of the correction and the growth of random noise during correction. Similar results were observed for the 19V and 22V channels. Fig. 3 shows the effect of observation set size on the correction at $\gamma$ = 0.5 while Fig. 4 shows the effect of varying the $\gamma$ on a 5×5 correction. To aid in the visualization of the results of the correction, the 37-GHz target image has been subtracted from each image to show only the differences remaining between the correction and the match image. A difference of less than 1 K is represented by a neutral grey which is predominant in the center and edges of Figs. 3(a) and 4(a). Lighter shades of grey indicate locations where the correction overestimates the temperature and darker shades of grey indicate locations where the correction underestimates the temperature.

Fig. 3 concentrates on the visual improvement seen by increasing the observation set size. As a reference, Fig. 3(a), shows the difference between the 19H and the 37H channels

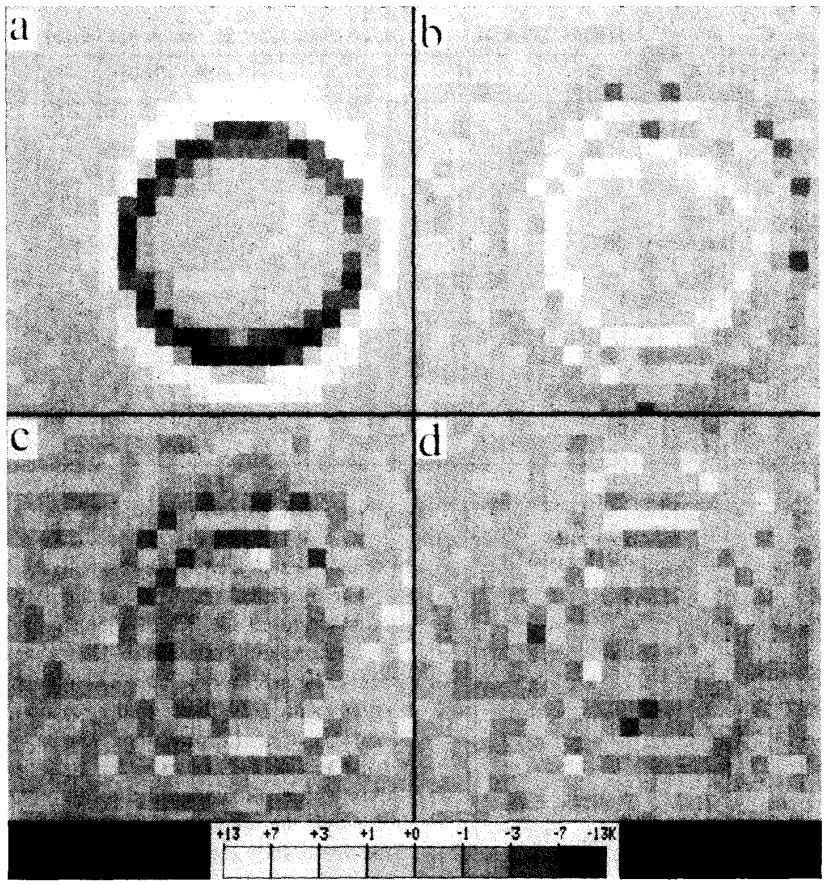


Fig. 3. Visual performance of the resolution correction as a function of observation set size for (a) no correction, (b) a 3×3 , (c) a 5×5 , and (d) a 7×7 observation set size. All corrections were made with noise conditioning held constant at $\gamma$ = 0.5. Each panel shows the difference between the corrected simulated scene as viewed by the 19H channel and the same scene viewed by the 37-GHz channel. A difference of less than 1 K is represented by a neutral grey. Lighter / darker shades indicate locations where the correction overestimates / underestimates the correct temperature. The range of brightness temperatures in (a) is about ± 20 K.

for the simulated circle feature prior to any correction. Due to the sharper 37-GHz antenna function, the 19H channel is warmer than the 37H in the area outside the feature edge and colder inside the edge with a maximum difference of 20 K. The random noise having occasional values up to 2 K can be seen in the flat field portions away from the feature edge. The 3×3 correction (Fig. 3(b)) shows a significant reduction of the difference between the 19H corrected and 37H target images. Concentric rings of alternating warm and cold deviations are seen around the feature edge, indicating incomplete correction. The 5×5 correction (Fig. 3(c)) does a very good job at reducing the resolution difference between the 19- and 37-GHz channels leaving little evidence of the original circular feature. The 7×7 correction (Fig. 3(d)), showed little visual improvement at the feature edge. Random noise can be seen to increase in the corrected images as larger excursions in temperature ( lighter and darker shades)

Fig. 4 focuses on the visual aspect of the noise as the error conditioning value, $\gamma$ is increased while the observation set remains fixed at 5×5. For reference, Fig. 4(a), like Fig. 3(a) shows the difference between the uncorrected 19H and 37H channels. Fig. 4(b) shows the 19H channel corrected with a 5×5 observation set and no noise conditioning. The noise component dominates this image with temperature fluctuations of more than 15 K, obscuring any uncorrected differences in the feature. When $\gamma$ is set at the optimum value of 0.5 (Fig. 4(c)), the noise is significantly reduced, revealing some remaining artifacts of the incomplete correction. At $\gamma$ = 2 (Fig. 4(d)), the noise is reduced further but the correction appears to be less complete.

The imagery results from the simulated data qualitatively confirm those obtained by the statistical tests. The results are used in the next section to guide the choice of the observation set size and noise conditioning to apply to the real data. The noise-conditioning factor used for the real data tests was chosen to obtain the minimum in the RMS difference with secondary consideration placed on reducing the noise component. This was done because the noise component was still significantly reduced at these points. The best observation set size for use in the real data tests is that of a 7×7 set.

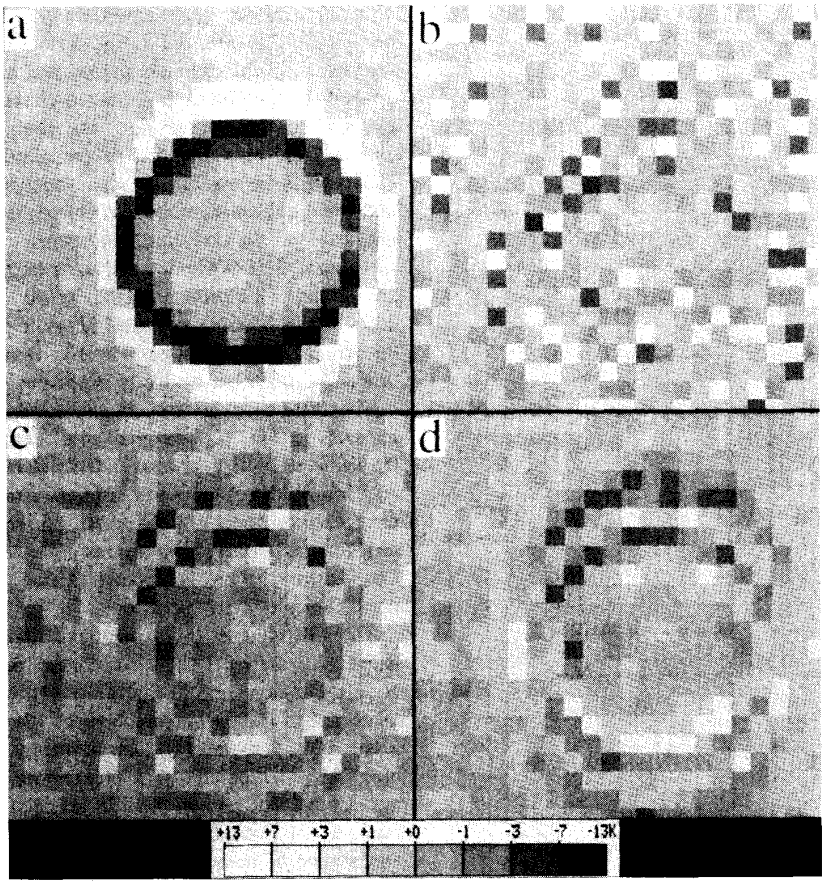


Fig. 4. Visual performance of the resolution correction as a function of noise conditioning for (a) no correction and (b) for a correction using a 5×5 observation set with the conditioning factor, $\gamma = 0$, (c) $\gamma = 0.5$, (d) and $\gamma = 2$. Each panel shows the difference between the corrected simulated scene as viewed by the 19H channel and the same scene viewed by the 37H channel.

For a number of reasons, the 5×5 set was chosen instead. First, little improvement in the statistics and the visual results were obtained in switching from the 5×5 to the 7×7 set. Second, the small improvements promised did not warrant the greatly increased computer time required to generate correction coefficients at the 7×7 size. On our VAX 11-780 computer, it takes about 5 min of CPU time to generate one 3×3 set of correction coefficients, about 20 min to generate a 5×5 set, and about 60 min to generate a 7×7 set. Third, as larger and larger observation sets are required, missing lines or bad data points affect larger surrounding areas in the final corrected data. Hence, only a 5×5 observation set will be tested with the real data. It should be emphasized that to a certain extent, the above decisions are arbitrary. For many purposes, a noise component of 1 or 2 K is acceptable. This may not be true for all applications.

As a final illustration of the enhancement achieved by this technique, Fig. 5 shows cross section of the 19-, 22-, and 85-GHz, vertically polarized response functions before and after the correction is applied. Results are shown for a pixel at the center of the scan, as well as near the edge. The 37-GHz response function is also shown for reference. The results show that the enhancement procedure has effectively increased the resolution (full width at half maximum) of the low frequency channels by roughly 15 km. While the match is by no means perfect, it clearly represents a significant improvement. The correction of the 85-GHz channel is almost perfect as expected.

## IV. Real SSM/I Data Results

Based on the discussion in the previous section, the coefficients for real SSM/I data correction are all generated on a 5×5 observation set with the following noise conditioning values: $\gamma$ (19H) = 0.5, $\gamma$ (19V) = 0.25, $\gamma$ (22V) = 1.0, $\gamma$ (85H) = 0.0, $\gamma$ (85V) = 0.0. Correction coefficients generated using this combination are applied to correct a real SSM/I data case containing sharp features such as coastlines to verify the simulation results. Verifying the correction for real data is primarily qualitative with examinations being made of the imagery and image differences.

Correcting the real data is very similar to correcting the simulated data. One major difference between the real and

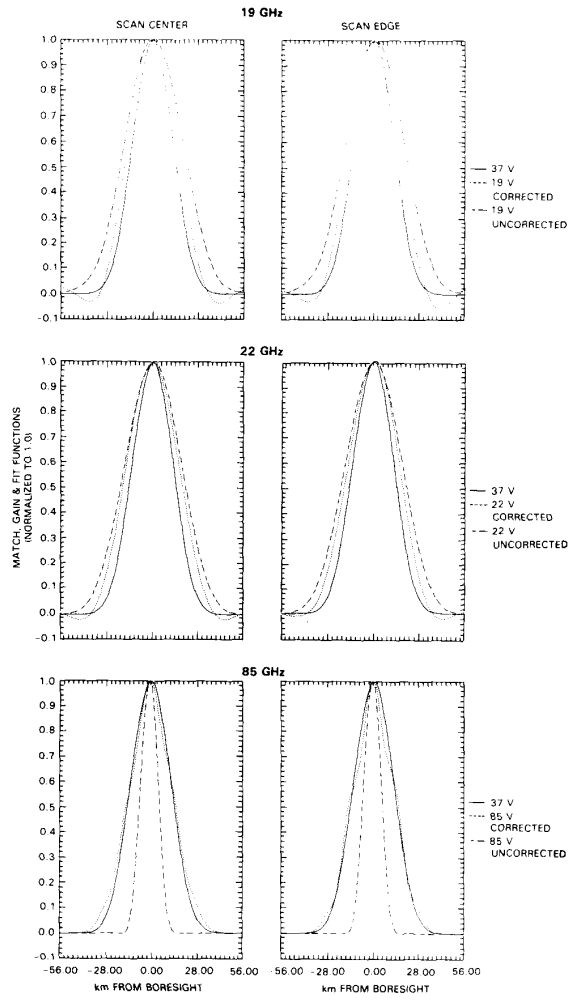


Fig. 5. Comparison of original response function, corrected response function and match function for the 19- , 22- , and 85-GHz vertically polarized channels. Panels on the left represent response functions at the center of the scan (pixel position 32 of 64), while the panels on the right represent response functions near the edge of the scan (pixel position 8 of 64). All response functions have been normalized to 1.0 to facilitate comparisons.

simulated data that will have to be watched is the relative locations of observations going into the observation set for the real data. The scan geometry of the SSM/I does not result in observations on a regular grid except in the center of the scan. At the sides of the scan, the grid pattern is deformed due to the conical scan geometry of the instrument. The altered relative positions of the observations to a central observation require that a new set of correction coefficients be used for each observation along a scan. In practice, this is only done for every fourth (eighth for the 85 GHz) observation being corrected due to the long amount of time it takes to generate a set of correction coefficients. This is a good approximation for intervening observations because the relative positions in the observation set change little over a small section of the scan.

The correction discussed above is applied to SSM/I data covering a portion of the southeast U.S. and Cuba on September 23, 1987 at 0000 UTC. Fig. 6 shows the scene viewed by the seven SSM/I channels before and after the correction is applied. Images of each corrected channel are placed beside the uncorrected channel for easy comparison. The 37-GHz channels are also included so comparisons to the corrected channel can be made. The scene contains a mixture of land and water so that the improvement of the resolution should be noticeable at the coastline. Numerous showers extend across the central Gulf of Mexico and some large thunderstorms exist around the east Florida coast. These storms can be most easily seen in the 85-GHz channels (Figs. 6(i), (k)) as the much cooler areas (bright spots), where substantial scattering of the upwelling radiation by ice is occurring.

The difference in resolution of each channel can clearly be seen in Fig. 6. The goal is to correct each channel to the same resolution as the 37-GHz channel (Figs. 6(g), (h)). As each SSM/I channel has different radiative properties, one cannot make direct comparisons against the 37-GHz channel to show the improvement as was done in the simulation tests. Consequently, there is no quantitative estimate of the best correction method for real data.

The 19H channel (Figs. 6(a) and (b)) and the 19V channel (Figs. 6(c) and (d)) show substantial correction in both the coastline regions and in the rain features. In particular, Lake Okeechobee stands out much more clearly in the corrected scene (Figs. 6(b) and (d)) than in the uncorrected scene (Figs. 6(a) and (c)). The clarity of this feature approaches but does not achieve that seen in the 37H scene (Fig. 6(g)). In general, random noise amplification is not noticeable except for the appearance of some mild banding in the corrected scene at the coastline. This more correlated noise which exists in the 19H and 19V channels may be eliminated by weighting the correction coefficients more strongly toward minimizing the error or by possibly correcting for the banding in the data prior to the resolution correction.

A cross section of the brightness temperatures was taken for the 19H channel to show the improved resolution of the coastline and small features. The cross section, indicated by a white line in Figs. 6(a) and (b) was made across the Florida peninsula, passing through Lake Okeechobee. Fig. 7 shows a plot of the brightness temperatures in this region (a) prior to and (b) after the correction. It can be seen that the visibility of Lake Okeechobee has increased significantly. The temperature in the lake was decreased by about 8 K due to the correction. Also, the Atlantic and Gulf coasts are more sharply delineated as shown by a slight increase in the gradient across the coastlines.

The 22V channel (Figs. 6(e) and (f)) shows a smaller degree of improvement than the 19-GHz channels as predicted by the simulation results (see Fig. 1(a) and Table II). This may be because the 22-GHz channel requires less correction in the first place due to the better match of the 22V to the 37V the antenna function. The lack of correction may also be due to the noise in this channel of 0.75 K which is greater than the 0.45 K noise in the 19-GHz channels. In general, the vertical polarization channels also offer less contrast in the features to improve upon. The 85H channel (Figs. 6(i), (j)) and the

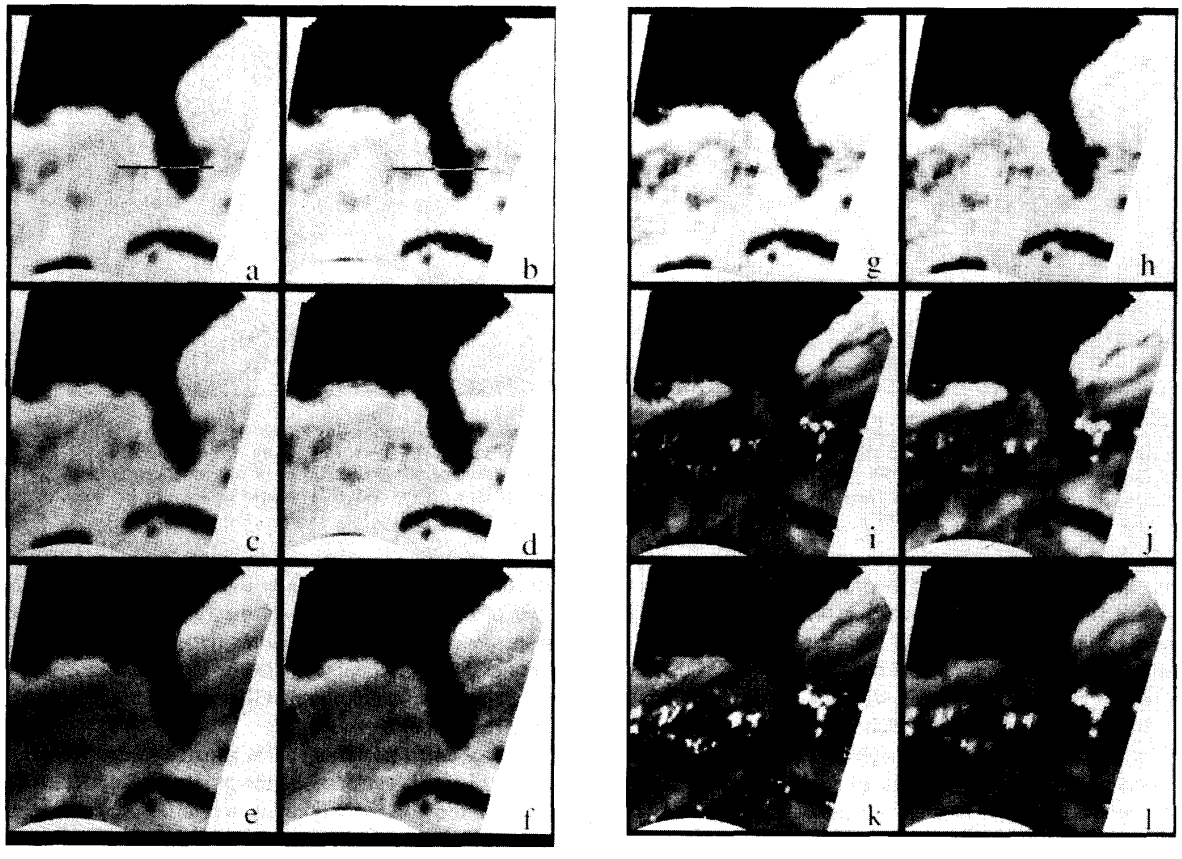


Fig. 6. Uncorrected and corrected SSM/I data taken over the southeast U.S. and Cuba on September 23, 1987 at 0000 UTC. The uncorrected channels: (a) 19H, (c) 19V, (e) 22V, (i) 85H, and (k) 85V are placed beside the resolution corrected versions: (b) 19H, (d) 19V, (f) 22V, (j) 85H, and (l) 85V. The optimum corrections were applied to make the corrected channels match the resolution of the (g) 37H or (h) 37V channels. Warm areas such as the Florida peninsula have darker grey shades while colder areas such as the surrounding ocean have lighter shades. The horizontal white lines in the 19H and V images indicate the location of brightness temperature cross sections shown in Fig. 6.

85V channel (Figs. 6(k) and (l)) show no adverse effects of the correction. This is not surprising as decreasing the resolution to the 37 GHz is an averaging process which decreases the noise in the data. Coastline features in the corrected 85H and V channels correspond well to their 37-GHz counterparts.

A second SSM/I image for which there is coincident radar data was examined in order to illustrate the correction results in a more quantitative way. Fig. 8(a) shows a Patrick Air Force Base radar image, taken at 00:04 UTC on January 25, 1988. A line of showers extending from east to west approximately 100 km north of Cape Kennedy can be seen in the image. A second raincell, which is very small, but containing intense rain up to 20 mm/h can also be seen off the coast of Florida, approximately 80 km east of Fort Lauderdale. This raincell is very interesting for our purposes on two accounts. First, higher elevation radar images (not shown here), indicate that this is a very shallow cell, not extending very far above the freezing level. This is also confirmed in the 85-GHz channel of the SSM/I, which shows only a very small decrease in brightness temperatures over this cell to approximately 255 K

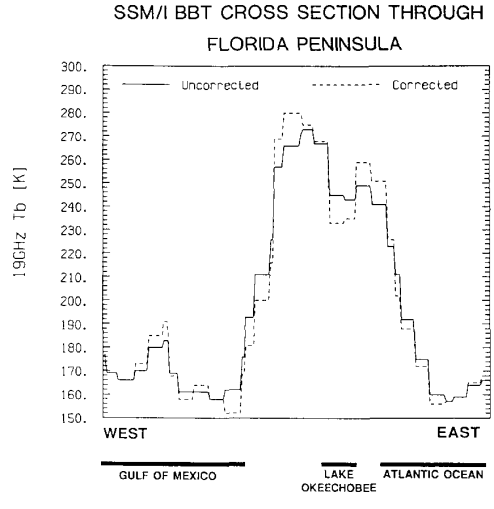


Fig. 7. SSM/I brightness temperature cross section through the Florida peninsula for the uncorrected (solid) and the corrected (dashed) 19H channel. The location of the cross section is indicated by a horizontal white line on Figs. 6(a) and (b).

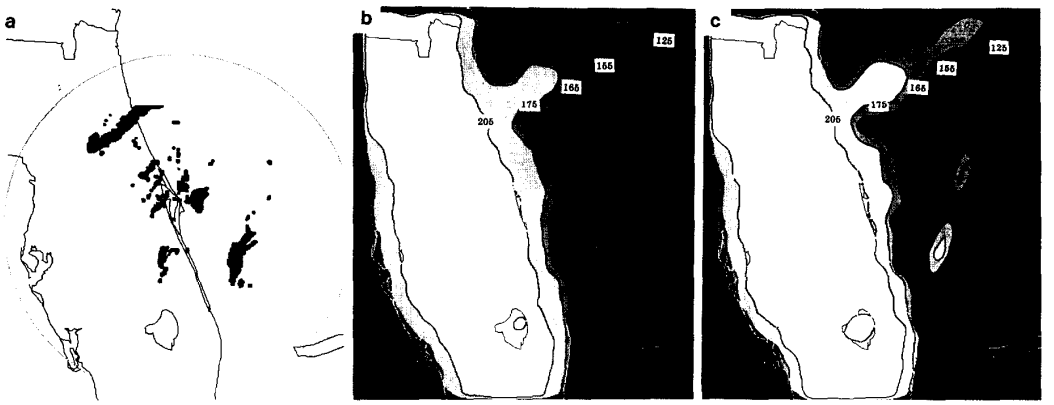


Fig. 8. Improvement of the resolution of small features as a result of resolution correction. (a) Patrick Air Force Base radar image of raincells around the Atlantic coast of Florida at 0004 UTC, on January 25, 1988. Reflectivity derived rainrates are shown as shaded areas with 1, 5, and 10 mm/h rainrate intensities. (b) Contoured SSM/I 19H image of the same area at the same time. The contours range from 125 to 205 K with 10 K intervals from 155 to 175 K. (c) Same data as (b) but for the corrected 19H channel.

from the 265 K background. Normally, convective raincells cause large brightness temperature depressions in the 85-GHz channel due to ice scattering. Any rainfall information for this cell must therefore come from the warming in the lower frequency channels associated with the thermal emission of the precipitating liquid. The small dimensions of the raincell, however, result in a very small signature in the 19H brightness temperatures. Contours of the brightness temperature field for the uncorrected 19H brightness temperatures are shown in Fig. 8(b). Fig. 8(c) shows the 19H brightness temperature contours after applying the resolution enhancement technique. The brightness temperature at the core of the raincell is seen to have increased by approximately 20 K. This is intuitively satisfying since a larger, better defined signal is what one would expect if the measurements were actually taken at a higher spatial resolution.

A way of quantitatively seeing the improvement brought about by the resolution enhancement technique, is to define the visibility of the feature as:

$$V = (I_2 - I_1)/(I_2 + I_1) \tag{11}$$

where I2 is the brightness temperature of the feature and I1 is a neighboring brightness temperature. For the 19H channel, the visibility of the feature was 0.044 before correction and 0.071 after correction. A lesser increase of visibility occurred in the 19V channel with V changing from 0.022 uncorrected to 0.038 corrected. The 22V channel showed only a slight improvement of from 0.012 to 0.014.

## V. Conclusions

In summary, we feel that the Backus and Gilbert approach produces adequate enhancement of the spatial resolution to make such a correction worthwhile. Results from Section III suggest that this technique decreases brightness temperature differences stemming solely from spatial resolution differences by over 50% for the low resolution channels. This is accomplished with only a modest increase in random noise. The correction can also help to better resolve small features which would otherwise be lost due to the lack of resolution. This can be important in making better retrievals of atmospheric quantities.This correction can also be used to average the 85-GHz channels to match the 37-GHz resolution when uniform spatial resolution is required.

The final correction coefficients adopted in this study use a $5\times5$ set of pixels surrounding the pixel to be corrected. The values for the noise conditioning weighting function, $\gamma$, are given explicitly for each channel in Section IV. These values were deemed most satisfactory for ongoing rainfall retrieval research. Because the values of $\gamma$ that were selected produce only a slight increase in random noise, however, we feel that the derived correction coefficients, $a_i$, should be of use to researchers in a variety of fields. As a necessary caution, however, it must be understood that the values of $\gamma$ in this paper were determined from simulated data and that it is therefore possible that better values of $\gamma$'s might be found for specific circumstances and applications using real data. This paper did not address the issue of finding the best possible $\gamma$'s from real data because that effort deals primarily with the validation of derived results and is therefore a quite separate topic.

## Acknowledgment

We wish to thank Harold Pierce and Lafayette Long for their assistance in preparing some of the images, as well as the reviewers for their thoughtful comments.

## References

[1] G. Backus and F. Gilbert, "Uniqueness in the inversion of inaccurate gross earth data," *Phil. Trans. Roy. Soc. London*, vol. A266, pp. 123–192, 1970.

[2] A. Stogryn, "Estimates of brightness temperatures from scanning radiometer data," *IEEE Trans. Antennas Propagat.*, vol. AP-26, pp. 720–726, 1978.

[3] J. Hollinger, R. Lo, G. Poe, R. Savage, and J. Peirce, "Special sensor microwave / imager user's guide," Naval Research Laboratory, Washington, DC, Dec. 14, 1987.
[4] G. Backus and F. Gilbert, "Numerical applications of a formalism for geophysical inverse problems," *Geophys. J. R. Astro. Soc.*, vol. 13, pp. 247–276, 1967.
[5] G. Backus and F. Gilbert, "The resolving power of gross earth data," *Geophys. J. R. Astro. Soc.*, vol. 16, pp. 169–205, 1968.

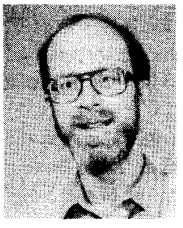

**Wayne D. Robinson** received the M.S. degree in meteorology from the University of Chicago in 1978.

Since then, he has worked with data from a variety of satellite-borne instruments at Goddard Space Flight Center, performing both research and software development. He was a member of the VAS Demonstration Project and is currently developing software for the Atmospheric and Oceanographic Information Processing System (AOIPS).

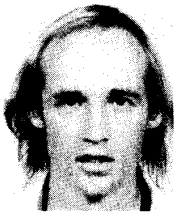

**Christian Kummerow** received the Ph.D. degree in physics from the University of Minnesota in 1987. His main research focus was radiative transfer in relation to remote sensing. After receiving the Ph.D., he went to Goddard Space Flight Center, where he has been working on rainfall monitoring from space by microwaave techniques. He is currently involved in prelaunch activities for the Tropical Rainfall Measuring Mission.

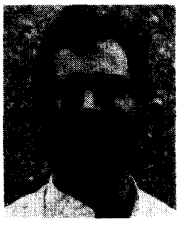

**William S. Olson** received the Ph.D. degree in meteorology from the University of Wisconsin-Madison in 1987.

Since then, he has worked as a researcher in satellite remote sensing and modeling applications in the Cooperative Institute for Meteorological Satellite Studies at the University of Wisconsin, where he is developing passive microwave retrieval methods for operational and research modes. His interests include radiative transfer, multisensor retrievals, image processing, data assimilation, and numerical weather prediction model applications.